



Microseismic source location method based on a velocity model database and statistical analysis

Bing-Rui Chen^{1,2} · Tao Li^{1,2} · Xin-Hao Zhu^{1,2} · Fan-Bo Wei^{1,2} · Xu Wang^{1,2} · Ming-Xing Xie³

Received: 29 March 2021 / Accepted: 19 August 2021 / Published online: 15 September 2021
© Saudi Society for Geosciences 2021

Abstract

Matching the velocity model to the actual engineering and geological conditions and improving the accuracy and stability of the microseismic (MS) source location remain challenges for scientists. An MS source location method based on a velocity model database and statistical analysis, named LM-VMD-SA, is proposed in this study. The method firstly divides the monitoring area into different subareas based on four influencing factors and creates an initial velocity model database by assigning an initial velocity to each sensor combination. Secondly, blasting tests are carried out in each subarea, where the velocity model database is inverted using a location error optimization method based on the pattern search algorithm (LEOM-PSA). The initial velocity model database for each subarea is updated by the velocity model database of the blasting events in the same subarea, and a velocity model database is constructed. Then, the velocity models for all sensor combinations of an MS event are called from the velocity model database for the corresponding subarea by matching the sensor combination of the MS event, and all corresponding solutions of the MS event are solved by the ND-N method. Finally, the three-dimensional coordinates of MS source are identified by utilizing the log-logistic (3P) distribution probability density function. According to blasting tests in the Beiminghe Iron Mine, the location accuracy of the proposed method is 20.88% and 18.24% higher than that of the traditional method and subarea method, respectively. The application of the proposed method to the Beiminghe Iron Mine revealed the illegal mining activities at -125 m and -155 m level, providing effective technical support for mineral resources protection and mining safety.

Keywords Rock mechanics · Microseismic source location · Velocity model database · Statistical analysis · Illegal mining

Introduction

Since the 1960s, microseismic (MS) monitoring techniques gradually applied to many deep mines and tunnels subjected to high in-situ stress (e.g., Tezuka and Niitsuma 2000; Milev et al. 2001; Hirata et al. 2007; Yang et al. 2007; Xu et al. 2015; Lu et al. 2015; Ma et al. 2015; Li et al. 2019; Xiao et al. 2019; Long et al. 2020). The MS event location accuracy directly

affects the calculation of radiant energy, the analysis of MS activity, and the warning of rockbursts. Accordingly, velocity models and MS source location methods, two key factors that affect the MS event location accuracy, have been extensively studied by scholars worldwide.

The uniform velocity model, a simplified velocity model that ignores the differences in the characteristics of rock masses, is widely used by most scholars (e.g., Li et al. 2007; Dong et al. 2019; Zhu et al. 2019; Wu et al. 2020) and MS equipment manufacturers, such as the Institute of Mine Seismology (IMS) in Australia (Shang et al. 2017) and Engineering Seismology Group (ESG) in Canada (Tang et al. 2015). However, a large amount of monitoring data shows that the rock mass velocity in the stratum is not uniform, especially in complex geological bodies such as jointed or faulted rock masses. On this basis, many scholars have conducted intensive researches on various velocity models (Falls and Young 1998; Wang and Ge 2008). In the 1970s, Lee and Lahr (1975) proposed a layered velocity model, which was then employed in earthquake location tasks to

Responsible Editor: Longjun Dong

✉ Tao Li
tli@mail.whrsm.ac.cn

¹ State Key Laboratory of Geomechanics and Geotechnical Engineering, Institute of Rock and Soil Mechanics, Chinese Academy of Sciences, Wuhan 430071, China

² University of Chinese Academy of Sciences, Beijing 100049, China

³ Beiminghe Iron Mine of Minmetals Hanxing Mining Co., Ltd., Wu'an 056300, Hebei, China

reflect the effect of geological structures. Crosson and Peters (1974) compared the location results from four-layer velocity model, double-layer velocity model, and single-layer velocity model and found that the location results varied slightly outside the sensor array. Besides, greater location accuracy was achieved in the double-layer velocity model within the sensor array, followed by the four-layer velocity model and the single-layer velocity model. Adam and Peter (2009) established a spatially variable seismic velocity model with passive tomography for relocating seismic events. Gesret et al. (2015) integrated the velocity model into a probabilistic earthquake location formulation, which was solved by a new Bayesian formulation. It can be seen that those method mainly adopted a layered velocity model for improving the MS source location accuracy. These layered velocity models have mainly been utilized in natural seismology and in oil and gas fracturing, where significant geological stratification is observed. However, it is inappropriate to apply such models to mining and tunneling projects, which has insignificant geological stratification, especially in monitoring areas with goafs and faults (Mu et al. 2021).

Some scholars modified the velocity model and proposed anisotropic velocity models for location tasks in which the propagation velocity of the vibration signal from the MS source to each MS sensor might be different (Aki et al. 1977; Mooney et al. 1998). However, MS sources may randomly appear in different directions, and thus, it is difficult to obtain accurate velocities in all directions through field tests which require a lot of works and material resources. To further simplify the calculation, study on anisotropic velocity model mainly focused on the choice of appropriate parametrization of the stiffness tensor, like the Thomsen parameter, which was usually designed to capture the influence of elastic anisotropy on a seismic signature (Grechka and Duchkov 2011; Li et al. 2013; Ma et al. 2020). However, these studies are mainly focused on the fields of oil and gas production. Feng et al. (2017) proposed a highly accurate method for locating MS events. This method used an anisotropic velocity model, rockburst event monitor, and particle swarm optimization to make the calculation more feasible and location more accurate. It was reasonable that the anisotropic velocity model proposed based on the rockburst event was applied to locate the MS events in the rockburst development process because of the same ray paths of the seismic waves from the MS events and rockburst event to MS sensor. However, whether the anisotropic velocity model could be applied to MS events in different regions needed further verification. After that, Feng et al. (2015) studied sectional velocity models in deeply buried tunnels and provided different velocities for the sensors in the cross sections of two rows of tunnels. These approaches achieved a good location result, but the effect of the complex geological conditions does not be taken into

account in their method. Due to the complex geological conditions in mines, the existing simplified velocity models are no longer able to meet the requirements of the high-precision location, and the inversion of the anisotropic velocity model required a lot of manpower and material resources. Moreover, the use of an anisotropic velocity model may induce instability of the solution and may even make the solution unachievable. Therefore, it is urgent to propose a velocity model, which can be apply to the actual geological conditions and is simple for inversion.

Iterative methods and swarm intelligence algorithms are widely used for many MS source location tasks, and the essence of these techniques is to solve the minimum value of the objective function constructed by the difference between the observed and theoretical arrival times. At the beginning of the twentieth century, the Geiger method was first proposed based on the Gauss-Newton formula (Geiger 1912). As this method needed to solve partial derivatives and inverse matrices, the solution was unstable and easily diverged. In the 1970s, Crosson (1976) proposed a joint inversion for the location of the source and velocity structure (known as the SHH algorithm), where the velocity was an unknown parameter. However, the solving process for the source parameters was easy to become unstable. Subsequently, Poliannikov et al. (2014) proposed a new method for simultaneously locating multiple seismic events in the presence of an uncertain velocity model. This method included absolute as well as relative event locations, without requiring known reference or master events. Dong et al. (2017) proposed a set of analytical solutions for AE/MS source location, which used the log-logistic (3P) distribution probability density function for statistical analysis. The method highlighted four advantages, including no iterative solution, no pre-measured velocity, no initially evaluated source coordinates, and no square root calculations. Peng and Wang (2019) presented a novel construction method for an arbitrary 3D velocity model and a targeted hypocenter determination method based on that velocity model, which significantly improved the location accuracy in underground mining compared with the widely used simplex and particle swarm optimization methods. These MS source location methods were studied mainly based on a certain number of P-wave or S-wave arrival times and commonly provided solutions with excellent accuracy and stability. However, due to the dependence of the algorithm, the influence of large arrival time errors, unstable sensor arrays, and so on, the MS source location solution is sometimes unstable, nonunique, or even poor using the above location methods. Therefore, it is necessary to combine the trigger sensors to deeply dig out the location information for improving the location accuracy of MS sources.

To address the above problems, an MS source location method based on a velocity model database and statistical analysis (the LM-VMD-SA method) is proposed. First, the

velocity model database is created and updated, thereby providing a velocity model for each sensor combinations of the MS event. Then, the log-logistic (3P) distribution probability density function is introduced to fit the location results of all sensor combinations, aiming to obtain an accurate and stable solution for the MS source. Compared with the traditional method and the subarea method, the LM-VMD-SA method divides the velocity model of mining engineering in more detail by inverting and updating the velocity of each sensor combination. For the same MS event, the LM-VMD-SA method combines the triggering sensors to obtain multiple location results, and uses statistical analysis to eliminate the instability of the first location results from the traditional method and the subarea method. Moreover, the blasting test data shows that the location accuracy of the LM-VMD-SA method is greater than that of the traditional method and the subarea method. Finally, the proposed method is applied to the Beiminghe Iron Mine in Hebei Province and excellent application results are exhibited.

Location error optimization method based on the pattern search algorithm

A key step to create the velocity model database is to invert the optimal uniform velocity model (Wang et al. 2010). For this purpose, a location error optimization method based on the pattern search algorithm (LEOM-PSA) is proposed. The LEOM-PSA method combines the Newton downhill with Newton-Raphson (ND-N) method for determining the MS source location (Li and Chen 2013).

ND-N method

The ND-N method is an excellent MS source location method. The Newton downhill method can provide an initial source location result, which is close to the true value. Then, the result from the Newton downhill method is set as the initial iteration value in the Newton-Raphson method for solving a more accurate location.

Newton downhill method

The objective function of the Newton downhill method can be expressed as by the following:

$$F(X) = F(x_0, y_0, z_0, t_0) = \sum_{i=1}^n r_i^2 \tag{1}$$

$$r_i = t_i - t_0 - T_i \tag{2}$$

$$T_i = \sqrt{(x_i - x_0)^2 + (y_i - y_0)^2 + (z_i - z_0)^2} / v_p \tag{3}$$

where t_0 is the seismic time, v_p is the P-wave velocity, and n is the number of sensors; (x_0, y_0, z_0) are the coordinates of the MS source, and (x_i, y_i, z_i) are the coordinates of the i -th sensor; t_i is the observed arrival time of the i -th sensor, T_i is the propagation time from the i -th sensor to the MS source, and r_i is the difference between the theoretical P-wave arrival time and observed P-wave arrival time at the i -th sensor.

The Newton downhill method uses $-\omega(\nabla F(X^n))^{-1}F(X^n)$ as the search direction, and the iterative formula is given by the following:

$$X^{n+1} = X^n - \omega(\nabla F(X^n))^{-1}F(X^n) \tag{4}$$

where X^n is the n -th iteration value and $F(X^n)$ is the objective function of the n -th iteration.

The range of ω is $\varepsilon_\omega < \omega \leq 1$, and ω should satisfy the following formula:

$$\|F(X^{n+1})\| < \|F(X^n)\| \tag{5}$$

The initial value of ω is set as 1, and ω is halved until the above formula is satisfied.

Newton-Raphson method

During the Taylor expansion, the Newton-Raphson method takes the second-order term into account and uses $-\left[\nabla^2 F(X^n)\right]^{-1} \nabla F(X^n)$ as the search direction. Therefore, the iterative formula is given by the following:

$$X^{n+1} = X^n - \left[\nabla^2 F(X^n)\right]^{-1} \nabla F(X^n) \tag{6}$$

The above formula can be expressed as follows:

$$\sum_{i=1}^n \left[\frac{\partial r_i}{\partial X_j} \frac{\partial r_i}{\partial X_k} + r_i \frac{\partial^2 r_i}{\partial X_j \partial X_k} \right] \delta X_j = - \sum_{i=1}^n \left[r_i \frac{\partial r_i}{\partial X_k} \right] \tag{7}$$

where δX is the correction of the source parameter.

The nonlinear least-square solution is expressed as follows:

$$\left[A^T A - (\nabla_X A^T) r \right] \delta X = A^T r \tag{8}$$

$$\text{where } A = \begin{pmatrix} \frac{\partial T_1}{\partial x_0} & \frac{\partial T_1}{\partial y_0} & \frac{\partial T_1}{\partial z_0} & 1 \\ \vdots & \vdots & \vdots & \vdots \\ \frac{\partial T_n}{\partial x_0} & \frac{\partial T_n}{\partial y_0} & \frac{\partial T_n}{\partial z_0} & 1 \end{pmatrix}, r = \begin{pmatrix} r_1 \\ \vdots \\ r_n \end{pmatrix}.$$

The iteration will continue until the objective function satisfies the allowable convergence error.

Location error optimization method based on the pattern search algorithm

In the rock engineering, the arrival time of the P-wave is easy to pick because it is the first to arrive. The P-wave and S-wave

may overlap, making it difficult to accurately pick the S-wave arrival time. Therefore, the arrival time of the P-wave is often used to solve for the location of the MS source.

Given a velocity v_p , the ND-N method can be used to solve for the source coordinates. The spatial error w can be expressed as the distance between the calculated source coordinates (x, y, z) and actual source coordinates (x_0, y_0, z_0) :

$$w = \sqrt{(x-x_0)^2 + (y-y_0)^2 + (z-z_0)^2} \tag{9}$$

In the above formula, each velocity v_p corresponds to a spatial error w . Due to the complex functional relationship between the velocity v_p and spatial error w , the derivative of the spatial error w cannot easily be solved. The pattern search algorithm is an algorithm that does not need to solve the derivative (Yosef and Bruce 1994). The algorithm searches the descent direction of the function along the coordinate axis or the given direction, and its essence is an iterative process of searching, detection, and advancing. Therefore, combined with the Equation (9), the minimum spatial error and the corresponding optimal uniform velocity model can be obtained by the pattern search algorithm. The method for solving the optimal uniform velocity model is named the location error optimization method based on the pattern search algorithm (LEOM-PSA), and the flowchart of this method is illustrated

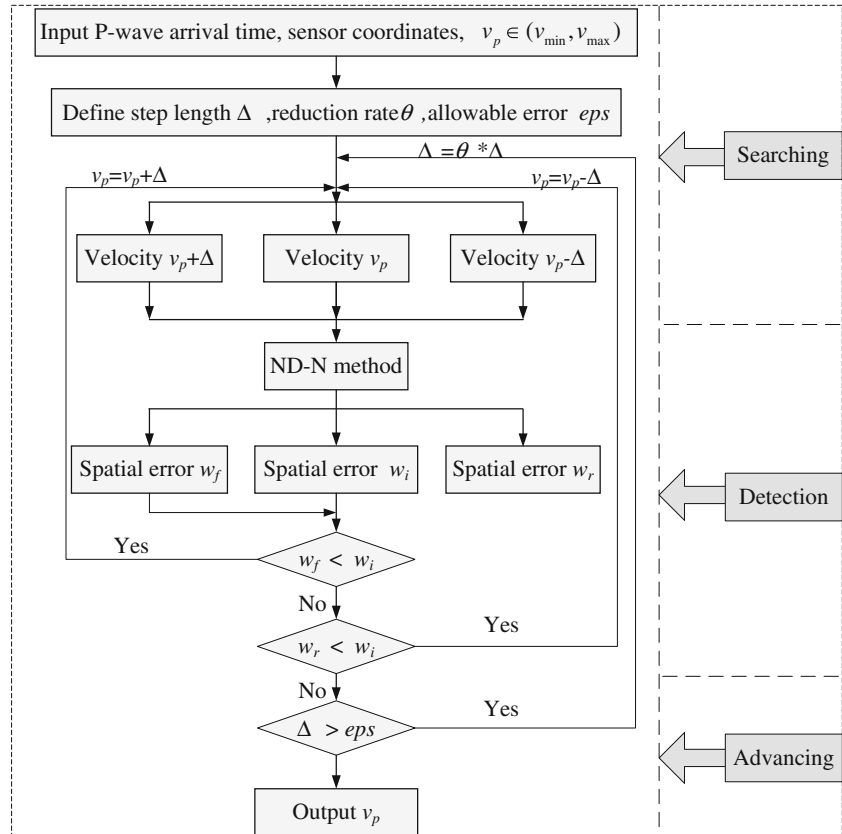
in Fig. 1. In the searching portion, two velocities, $v_p - \Delta$ and $v_p + \Delta$, are selected on both sides of the initial velocity v_p , then the spatial errors w_f, w_i , and w_r corresponding to the three velocities $v_p + \Delta, v_p$, and $v_p - \Delta$ are calculated. In the detection portion, the velocity corresponding to the minimum spatial error is obtained by comparing the spatial errors w_f, w_i , and w_r . In the advancing portion, the descent direction of the objective function is determined, and the initial velocity is updated until the convergence condition is reached.

MS source location method based on a velocity model database and statistical analysis

Velocity model database

To mimic the geological conditions in actual engineering and improve the MS source location accuracy, a velocity model database is proposed in this study. The database consists of many subarea velocity models, which are built adaptively by assigning different optimal uniform velocities to different sensor combinations. Different optimal velocity models are used for different MS source locations and triggered sensor combinations. A schematic diagram of the velocity model database

Fig. 1 Flowchart of the LEOM-PSA method



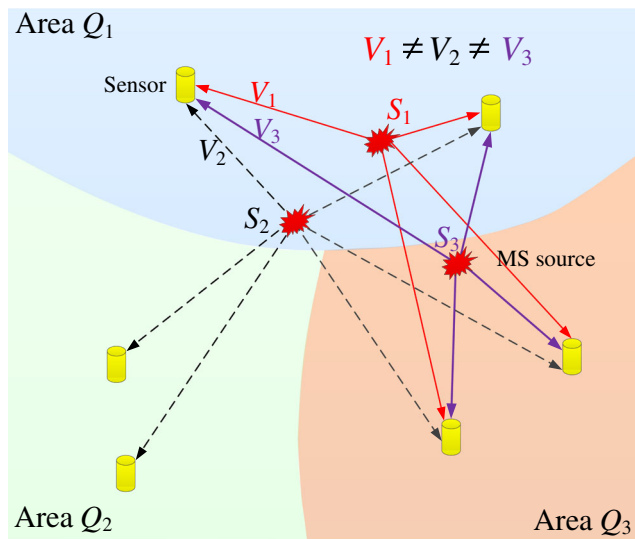


Fig. 2 Schematic diagram of the velocity model database

is presented in Fig. 2. Note that MS sources, S₁ and S₂, trigger different sensor combinations in the same subareas, which have different propagation directions and require different velocity models. Moreover, MS sources, S₁ and S₃, trigger the same sensor combination in different subareas, which also have different propagation directions and require different velocity models. Although the velocity model database is not a complete anisotropic velocity model, it considers the rock mass difference in the monitoring area formed by different sensor combinations. Furthermore, the velocity model database is easier to invert than the anisotropic velocity model due to the reduction of velocity parameters.

Method for creating the initial velocity model database

When creating a velocity model database, the whole monitoring area needs to be divided into several subareas according to its geological characteristics. Four factors need to be considered in the subarea division: (1) the priority areas that need to be focused on in an engineering project, such as areas with high geostress where intensive rockburst events are frequently detected; (2) areas with significant differences in the rock mass characteristics; (3) areas with many goafs and developed faults; and (4) the location relationship between the engineering monitoring area and the sensor array.

When $n \geq 4$ sensors are installed over the monitoring area, the number of combinations of k sensors among all n sensors is determined by C_n^k . Because at least 4 sensors need to be triggered to locate the MS source, k must satisfy $4 \leq k \leq n$. Assuming that n sensors can be triggered by the MS source in each subarea, the number of sensor combinations in each subarea is $C_n^4 + C_n^5 + \dots + C_n^k + \dots + C_n^n$. In this way, the initial velocity model database for each subarea can be created by

assigning a uniform velocity model (an empirical velocity model) and a large spatial error to each sensor combination. When the velocity model database in each subarea is initiated, an initial velocity model database for the whole monitoring area is created.

Method for updating the velocity model database

After the MS monitoring system is commissioned successfully, it needs to be tested by blasting events. For wave velocity inversion, several locations of blasting test need to be selected in each subarea, and their MS information is recorded. Then, assuming that m sensors are triggered in each blasting event, the number of sensor combinations of the blasting event is determined by $C_m^4 + C_m^5 + \dots + C_m^m$. Afterward, the LEOM-PSA method is used to invert the optimal uniform velocity model v_p of each sensor combination, aiming to create the velocity model database of the blasting events.

The velocity model database of each subarea is updated by the velocity model database of blasting events in the corresponding subarea. The flowchart for updating the velocity model database of the subarea is shown in Fig. 3. The spatial error reflects the quality of velocity inversion of the sensor combination. The velocity obtained by inversion is more consistent with the actual velocity in the monitoring area formed by the sensor combination when a smaller spatial error is obtained. Therefore, after the sensor combination of the

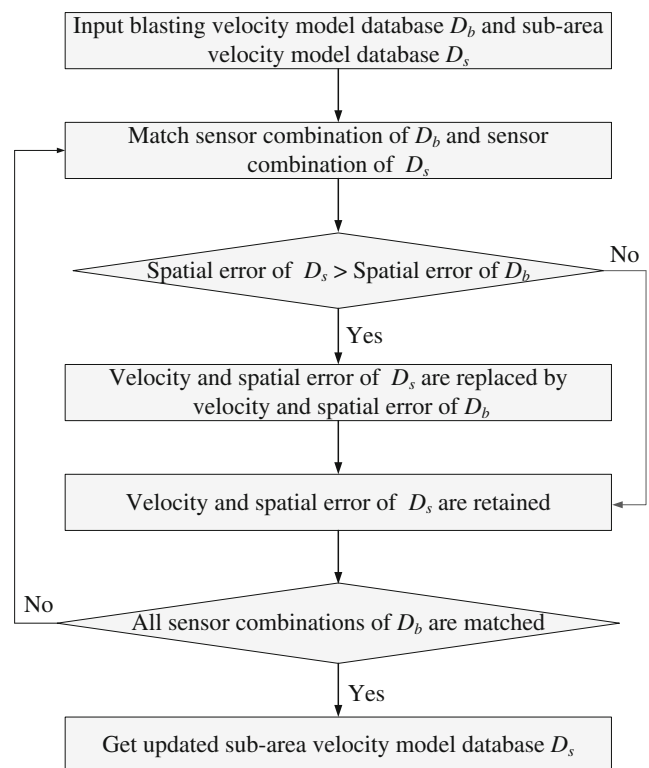


Fig. 3 Flowchart for updating the velocity model database of the subarea

blasting velocity model database and the sensor combination of the subarea velocity model database is matched, their corresponding spatial errors are compared. When the spatial error of the blasting velocity model database is less than that of the subarea velocity model database, the velocity and spatial error of the subarea velocity model database can be replaced by that of the blasting velocity model database. On the contrary, the spatial error and velocity of the subarea velocity model database are retained. After all sensor combinations of the blasting velocity model database are matched, the updating process of the velocity model database of the subarea is finished.

Microseismic source location method based on a velocity model database and statistical analysis

After the velocity model database is created and updated, the coordinates of the MS sources can be solved by the ND-N method based on the proposed velocity model database. Firstly, m triggering sensors are combined to obtain $C_m^4 + C_m^5 + \dots + C_m^m$ sensor combinations. Secondly, the match between the sensor combination of MS events and the sensor combination of the subarea velocity model database is performed. The velocity of the subarea velocity model database is provided to the ND-N method for event location, and $C_m^4 + C_m^5 + \dots + C_m^m$ location results are obtained. Then, all location results are divided into sets of x -coordinates, y -coordinates, and z -coordinates, and the 3σ criterion proposed by Dai and Wang (1992) are used to eliminate abnormal values of the three-dimensional coordinates. Finally, the filtered x -coordinate, y -coordinate, and z -coordinate sets are statistically analyzed. Dong et al. (2017) compared and analyzed more than 60 commonly used probability density functions and found that the log-logistic (3P) distribution probability density function is best for determining MS source locations. Therefore, the log-logistic (3P) distribution probability density function is introduced to fit the three-dimensional coordinates of the MS source. The coordinates corresponding to the maximum value of probability density considered as are the x -coordinate, y -coordinate, and z -coordinate of the MS source. This location method is referred to as the MS source location method based on a velocity model database and statistical analysis (LM-VMD-SA). The flowchart of the LM-VMD-SA method is shown in Fig. 4.

Verification

Test setting up

The Beiminghe Iron Mine in Hebei Province covering an area of 209,500 m² began production in 2002, having a designed annual production of 1.8 billion kg of

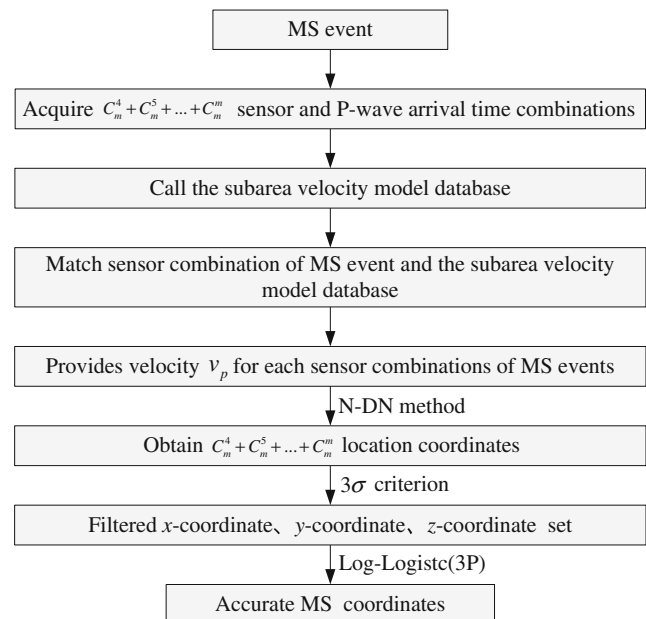
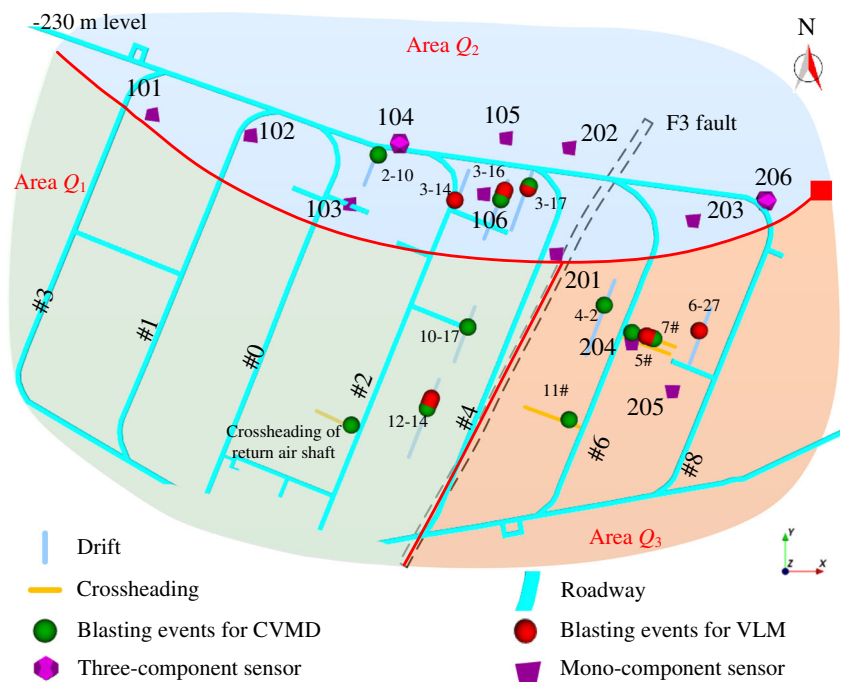


Fig. 4 Flowchart of the LM-VMD-SA method

iron ore. The height of the level is 60 m and the height of each sublevel is 15 m. The deposit is formed in the contact zone between Yanshanian diorite and Ordovician limestone. The ore mainly consists of magnetite, and the roof and floor of the ore body are limestone and diorite, respectively. The ore body has a length of 1620m, width ranging 92m from 376m, and depth ranging 134m from 679m. The geological structure in mines mainly consists of folds and faults. The density of ore is 3910 kg/m³ and the density of rock mass is 2710 kg/m³. The factor of loose is 1.6, and the hardness coefficient of ore ranges 8 from 12. A large F3 fault locates between the MB4 exploration line and the MB5+25 exploration line in the east of the ore body (Fig. 5), which has a compression-torsional fault with attitudes of NW307°∠65°, a vertical slip of 8.9m, and a horizontal slip of 17m. A fault zone with a thickness of about 8m locates near the fault, in which the rocks are broken. The sound of abnormal blasting is frequently heard by the workers at the substation on the -122 m level and the excavation roadway at the -185 m level since 2017. It indicates that cross-border illegal mining is taking place. The regional hydrogeological conditions of the Beiminghe Iron Mine are complex, and cross-border illegal mining may potentially lead to catastrophic consequences such as water inrush events, roof collapse, or floor collapse.

To solve the above problems and mitigate potential safety hazards, a 16-channel SinoSeism (SSS) MS monitoring system jointly developed by the Institute of Rock and Soil Mechanics, Chinese Academy of Sciences, and Hubei Seaquake Technology Co., Ltd., is deployed. The MS monitoring system consists of a 32-bit A/D acquisition apparatus,

Fig. 5 Distributions of the sensors, blasting points, and subareas in the monitoring area (creating velocity model database is shortened as CVMD, and verifying the LM-VMD-SA method is expressed as VLM)



moving coil sensors with a sensitivity of 100 V/ms^{-1} , and a PTP high-precision time synchronization server, as shown in Fig. 6.

Since main mining roadway locates above the -230 m level of the mine, normal construction can be affected by the sensor installation. Because the existence of deep silt and extensive water, the roadway at the -245 m level has difficulty in drilling holes and installing sensors. Therefore, a total of 10 mono-component sensors and 2 three-component sensors are arranged at the -230 m level. Because illegal mining activities generally take place in the north and southeast of the mining area, the sensors are arranged primarily along the upper haulage roadways, roadways No. 6 and No. 8 of the mining area, as shown in Fig. 5. The coordinates of the sensors are listed in Table 1.

The monitoring area is divided into three subareas, shown in Fig. 6, according to the location of the sensor array and the location of the faults. Areas Q_1 and Q_3 are outside the sensor

array and separated by the F3 fault, while area Q_2 is inside the sensor array. Ten blasting test points are deployed in 3 subareas to create and invert a velocity model database for each subarea, and the locations and blasting numbers of these points are shown in Fig. 6 and Table 2, respectively. The blasting tests are single-hole blasting tests with a small charge at each blasting test point. To verify the LM-VMD-SA method, 10 blasting events are carried out from September 27 to October 15, 2018 (Fig. 6 and Table 2), and the blasting location, time, waveform, and other data are recorded.

Creating and updating the velocity model database

The process of creating the velocity model database in area Q_1 is described as follows. First, 12 sensors are combined to obtain 3797 sensor combinations. The initial velocity model and spatial error of each sensor combination are assumed to be

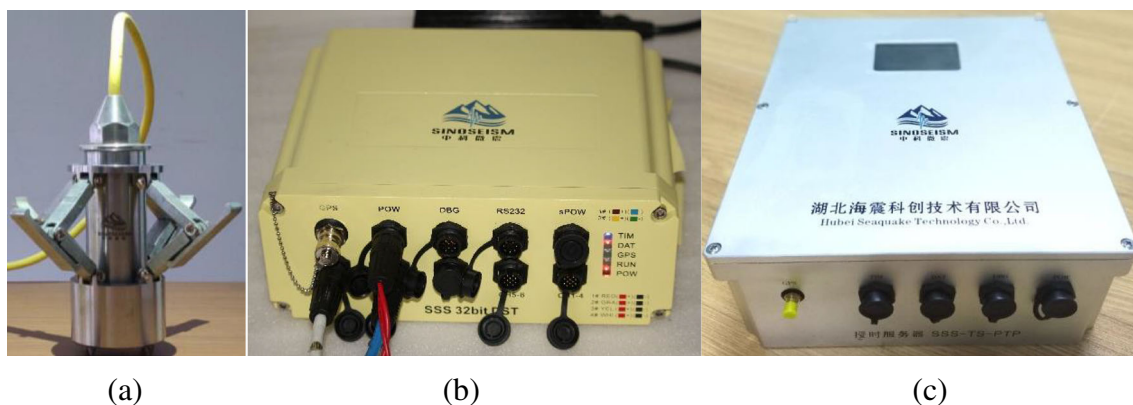


Fig. 6 The SSS MS monitoring system. **a** Sensor. **b** Acquisition apparatus. **c** Time synchronization server

Table 1 Coordinates of the sensors

No.	Coordinate (m)			No.	Coordinate (m)		
	x	y	z		x	y	z
101	1599.54	8771.51	-245.77	201	1956.15	8646.69	-235.43
102	1688.85	8749.96	-226.38	202	1965.26	8737.80	-218.34
103	1775.20	8690.28	-230.48	203	2075.01	8675.53	-229.89
104	1818.63	8743.12	-227.06	204	2020.12	8567.80	-221.69
105	1912.76	8750.27	-244.76	205	2057.23	8526.09	-231.02
106	1892.18	8699.04	-230.23	206	2138.42	8693.26	-230.23

5500 m/s and 100 m, respectively, and the initial velocity model database is created in area Q_1 . Similarly, initial velocity model databases of areas Q_2 and Q_3 are also created.

The velocity model database of the blasting event is the key to update the velocity model databases in the subareas, so optimal uniform velocity models for the sensor combinations of the blasting event should be solved first. The first blasting event of blasting test point No. 2, which triggers 11 sensors in area Q_1 , is taken as the example for inverting the optimal uniform velocity models and introducing the LEOM-PSA method. The parameters of the LEOM-PSA method are set as follows. The initial velocity v_p is 5500 m/s, the initial step length Δ is 20 m/s, and the reduction rate θ is 0.2; the velocity

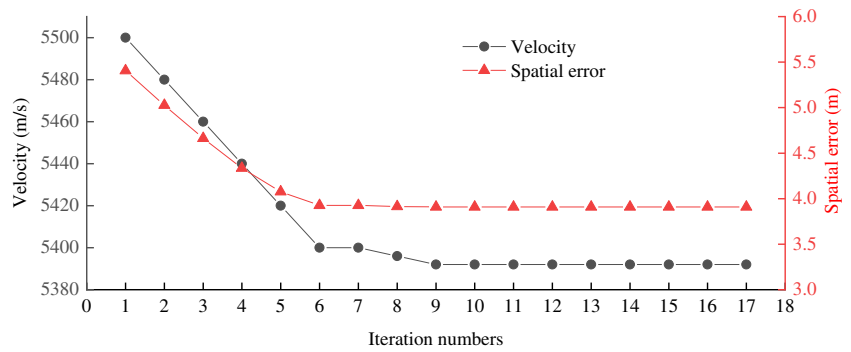
solution ranges from 4000 to 7000 m/s, and the allowable error ϵ_{ps} is set as 10^{-4} m. Fig. 7 depicts the variation in the velocity and the spatial error of the first blasting event at blasting test point No. 2 with the number of iterations during the solution process of the LEOM-PSA method. With the decrease of the location error, the velocity gradually stabilizes. When the number of iterations reaches 6, the LEOM-PSA method converges. The optimal uniform velocity is 5392 m/s, and the corresponding spatial error is 3.91 m. The same optimal uniform velocity is obtained, and the number of iterations is 3001 when using the enumeration method with the step length of 1 m/s. These results confirm the effectiveness and robustness of the LEOM-PSA method in acquiring accurate velocity.

Similarly, the optimal uniform velocity models for all sensor combinations of 13 blasting events in area Q_1 are solved based on the LEOM-PSA method, and the velocity model database of each blasting event is obtained. According to the updating procedure mentioned above, the initial velocity model database is updated by the velocity model databases of 13 blasting events in area Q_1 , and the velocity model database D_{11} of area Q_1 is obtained. The partial velocity model database of area Q_1 is shown in Table 3. The optimal uniform velocities and spatial errors are different for different sensor combinations in the same area. The velocity models of different sensor combinations describe the properties of rock masses in

Table 2 Locations of the blasting test points and blasting events

No	Site	Area	Coordinate/m			Blasting numbers	Function
			x	y	z		
1	12–14 drift	Q_1	1844.19	8516.79	-212	4	Creating the velocity model database
2	12–14 drift	Q_1	1845.16	8519.20	-212	5	
3	12–14 drift	Q_1	1845.98	8521.24	-212	4	
4	3–16 drift	Q_2	1906.93	8696.39	-198	4	
5	3–17 drift	Q_2	1927.97	8700.44	-198	5	
6	3–16 drift	Q_2	1907.93	8698.90	-198	3	
7	3–14 drift	Q_2	1865.68	8690.47	-198	4	
8	6–27 drift	Q_3	2073.15	8579.18	-198	3	
9	7 crossheading	Q_3	2028.46	8574.56	-198	6	
10	7 crossheading	Q_3	2032.51	8573.11	-198	5	
1	12–14 drift	Q_1	1842.45	8512.47	-212	1	Verifying the LM-VMD-SA method
2	10–17 drift	Q_1	1876.68	8582.30	-198	1	
3	Crossheading of return air shaft	Q_1	1777.13	8498.07	-212	1	
4	3–17 drift	Q_2	1928.76	8702.41	-198	1	
5	3–16 drift	Q_2	1904.78	8691.06	-198	1	
6	2–10 drift	Q_2	1800.64	8729.04	-198	1	
7	7 crossheading	Q_3	2034.44	8572.42	-198	1	
8	5 crossheading	Q_3	2018.63	8577.67	-213	1	
9	4-2drift	Q_3	1994.13	8599.20	-213	1	
10	11 crossheading	Q_3	1964.59	8502.65	-213	1	

Fig. 7 Evolution of the velocity and spatial error of the first blasting event at blasting test point No. 2 with the number of iterations based on the LEOM-PSA method.



different areas, which are set as average value of the velocity field in the monitoring area formed by the sensor combination for the convenience of inversion. Similarly, the initial velocity model database of area Q_2 is updated by the velocity model databases of 16 blasting events in area Q_2 , and the velocity model database D_{21} of area Q_2 is created. Likewise, the initial velocity model database of area Q_3 is updated by the velocity model databases of 14 blasting events in area Q_3 , and the velocity model database D_{31} of area Q_3 is also acquired

Fig. 8 shows the updating procedure of the velocity models of the sensor combinations. It can be seen that the spatial errors of the sensor combinations tend to be smaller with an increase in the number of updates. Generally, the spatial errors are closely related to the quality of the velocity model, and smaller spatial errors correspond to a greater velocity model, which can highly reflect the actual geological structure (Wang et al. 2010). In Fig. 8a–c, the velocities of the 2937th sensor combination in areas Q_1 , Q_2 , and Q_3 are 5639 m/s, 4852 m/s,

and 5201 m/s, respectively. The velocities of the same sensor combination vary among different subareas. It can be seen in Fig. 8a, d that the velocities of the 2937th sensor combination in area Q_1 and the 2060th sensor combination in area Q_1 are 5639 m/s and 5343 m/s, respectively. It can be concluded that the velocities of different sensor combinations in the same subarea are also different. Therefore, it is necessary to create a velocity model for each sensor combination.

Although the spatial error of a given sensor combination tends toward a smaller value with an increase in the number of updates, the adapted velocity model database needs to be checked in regular intervals, especially for the varied engineering and geological conditions.

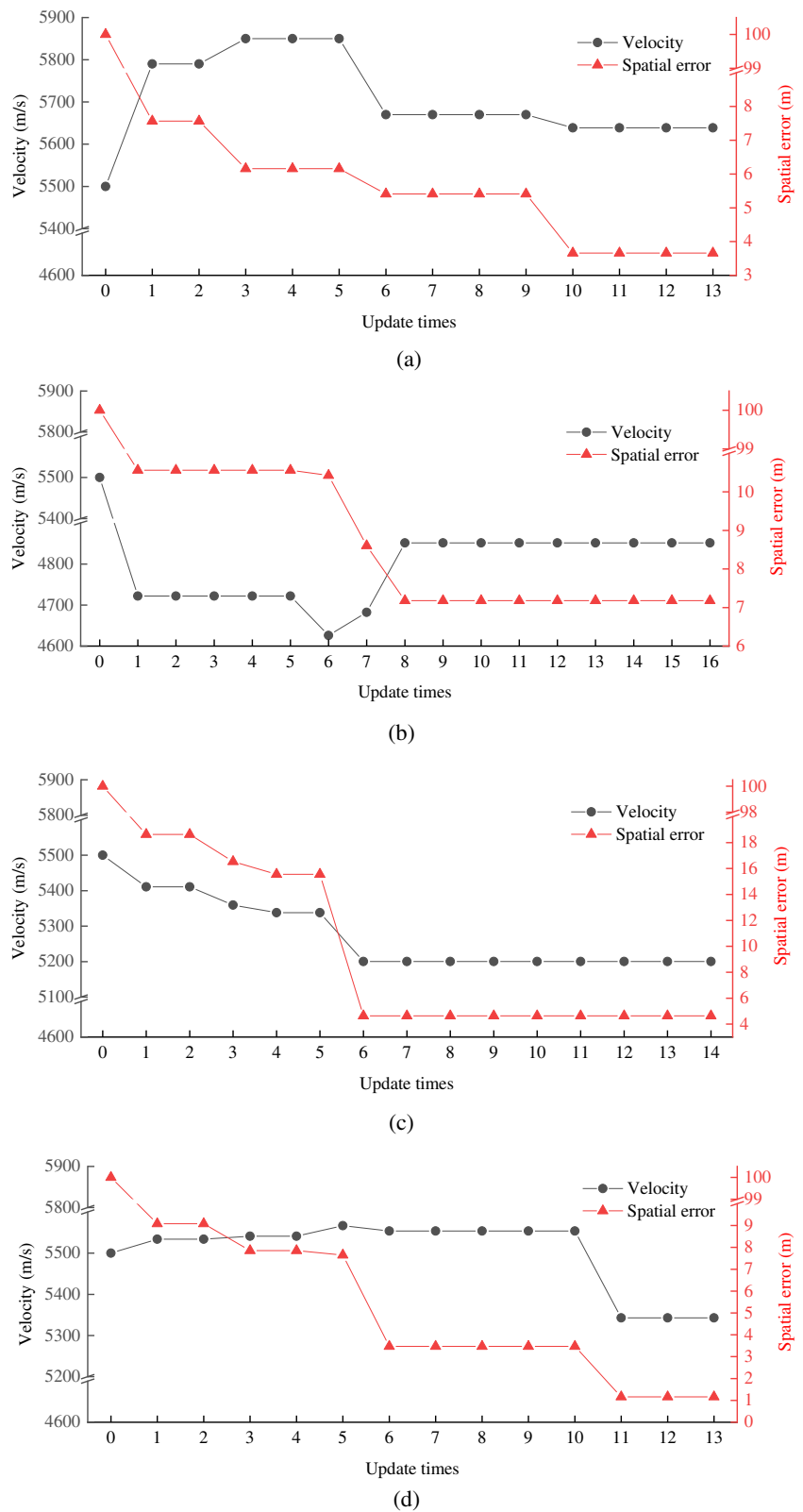
Verification of the LM-VMD-SA method

Blasting event No. 7, which triggers 8 sensors in area Q_3 , is taken as an example to illustrate the solution process of the

Table 3 Partial velocity model database of area Q_1

No.	Sensor combinations	Velocity (m/s)	Error (m)
49	101; 103; 104; 202	5457	15.61
50	101; 103; 104; 203	5328	15.50
693	101; 103; 202; 204; 205	5173	10.47
694	101; 103; 202; 204; 206	5166	4.84
1607	101; 103; 106; 203; 205; 206	5116	1.62
1608	101; 103; 106; 204; 205; 206	5199	3.36
2550	101; 103; 105; 106; 203; 204; 205	5271	2.84
2551	101; 103; 105; 106; 203; 204; 206	5211	1.25
3292	101; 103; 106; 201; 202; 203; 204; 206	5593	7.24
3293	101; 103; 106; 201; 202; 203; 205; 206	5488	5.65
3622	101; 103; 104; 105; 106; 201; 202; 204; 205	5436	7.63
3623	101; 103; 104; 105; 106; 201; 202; 204; 206	5250	2.44
3764	101; 103; 104; 105; 106; 201; 202; 203; 204; 205	5250	1.69
3765	101; 103; 104; 105; 106; 201; 202; 203; 204; 206	5169	1.07
3795	101; 103; 104; 105; 106; 201; 202; 203; 204; 205; 206	5220	1.04
3796	102; 103; 104; 105; 106; 201; 202; 203; 204; 205; 206	5058	27.63
3797	101; 102; 103; 104; 105; 106; 201; 202; 203; 204; 205; 206	5434	28.69

Fig. 8 Updating of velocity models for different sensor combinations. **a** The 2937th sensor combination in area Q_1 . **b** The 2937th sensor combination in area Q_2 . **c** The 2937th sensor combination in area Q_3 . **d** The 2060th sensor combination in area Q_1 (the 2937th sensor combination includes sensor Nos. 103, 104, 201, 202, 204, 205, and 206; the 2060th sensor combination includes sensor Nos. 103, 104, 201, 202, 204, and 205)



LM-VMD-SA method. Firstly, 163 sensor combinations are produced based on the 8 triggered sensors. Secondly, the velocity model of the corresponding sensor combination is

called in the velocity model database of area Q_3 , and 163 solutions are obtained by the ND-N method. Thirdly, large deviations in the x -coordinate, y -coordinate, and z -coordinates

are filtered out by the 3σ criterion, and the probability densities of the x -, y -, and z -coordinates of the 163 solutions are fitted utilizing the log-logistic (3P) distribution probability density function, shown in Fig. 9. Finally, the coordinates corresponding to the maximum probability density are considered as the x -coordinate, y -coordinate, and z -coordinates of blasting event No. 7. The x -coordinate, y -coordinate, and z -coordinates of blasting event No. 7 are 2044.51 m, 8570.25 m, and -190.54 m, and their errors are -10.07 m, 2.17 m, and -7.46 m, respectively.

As shown in Fig. 9, the spatial errors mainly range from -20 m to 20 m in three directions of the same blasting event. The spatial errors come from the arrangement of sensor array, arrival time error, and algorithm dependence. The accuracy and stability of the solution are greatly affected when only one sensor combination is adopted. This is the main reason why the statistical analysis is introduced.

In the same way, 10 blasting events are located by the LM-VMD-SA method. All solutions converge during the solution process, and the results are shown in Figs. 10 and 11. The average location errors of the blasting events in areas Q_1 , Q_2 , and Q_3 are 21.19 m, 13.69 m, and 19.12 m, respectively. Area Q_2 has the smallest average location error and closest distance to the center of the sensor array, followed by areas Q_3 and Q_1 . Previous studies also reveal that a smaller location error is acquired when the MS source is closer to the center of the sensor array (Li et al. 2014). Therefore, the relative distance between the sensor array and monitoring area should be taken into account when the MS monitoring scheme is designed.

To verify the superiority of the LM-VMD-SA method, 10 blasting events are located by a traditional method (Li and Chen 2013) with a uniform velocity model and a subarea method (Feng et al. 2015). The velocity is set to 5222 m/s in uniform velocity model, and three different velocities, i.e., 5384 m/s, 5124 m/s, and 5247 m/s are set for areas Q_1 , Q_2 , and Q_3 in subarea method. Comparisons of the location results among the traditional method, the subarea method, and the LM-VMD-SA method are shown in Fig. 11. The average location errors of the traditional method, the subarea method, and the LM-VMD-SA method are 22.89 m, 22.15 m, and 18.11 m, respectively, in the three subareas. The location accuracy of the LM-VMD-SA method is 20.88% higher than that of the traditional method and 18.24% higher than that of the subarea method. Therefore, the LM-VMD-SA method therefore achieves higher accuracy and better stability than both the traditional method and the subarea method.

Field applications

Illegal mining activities in the north and southeast of the mining area of the Beiminghe Iron Mine are mainly focused. From October 17, 2018, to April 30, 2019, a total of 5396

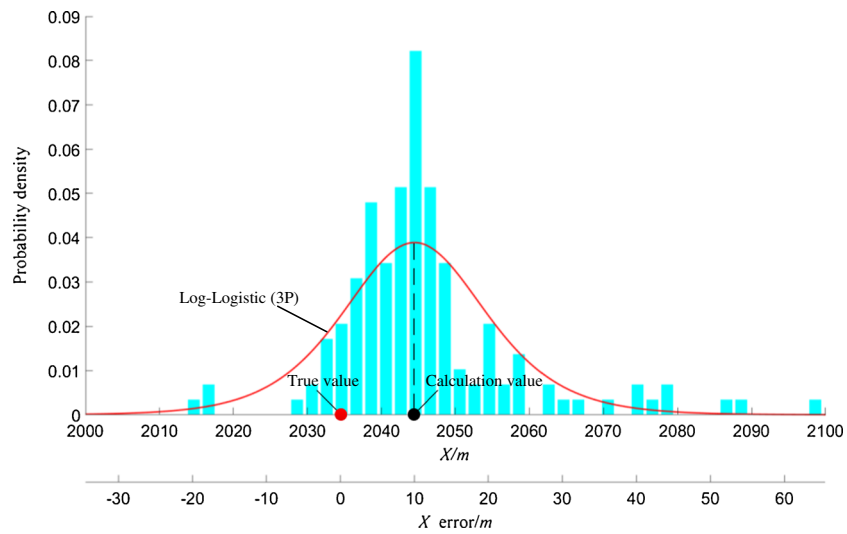
blasting events were monitored by the MS monitoring system, and 478 abnormal blasting events were extracted based on the blasting records. Based on the velocity model databases of areas Q_1 , Q_2 , and Q_3 , abnormal blasting events are located by the LM-VMD-SA method, and their locations are shown in Fig. 12. It reveals that abnormal blasting events are mainly concentrated in the suspicious areas No. 1 and No. 2. Suspicious area No. 1 is located in area Q_3 , while suspicious area No. 2 is located the north of the mining area and about 100 m away the boundary of the Beiminghe Iron Mine.

According to the MS monitoring results, several boreholes are drilled in the suspicious area No. 1. In situ borehole information reveals that illegal mining roadways are found to be located at -125 m level and -155 m level, shown in Fig 12b. Besides, some equipments are found on the -125 -m level illegal mining roadway. It indicates that the determined location of the illegal mining roadways by the MS monitoring is constant with the actual illegal mining activity in mines. Although the monitored suspicious area No. 2 is about 100 m away from the boundary of the Beiminghe Iron Mine, it indicates the illegal mining activity may occur in the future. Thus, it is necessary to increase the number of sensors and strengthen the monitoring in the upper part of the mining area. These findings confirm that the LM-VMD-SA method is feasible for engineering applications. This method can provide support for mineral resources protection and mining safety.

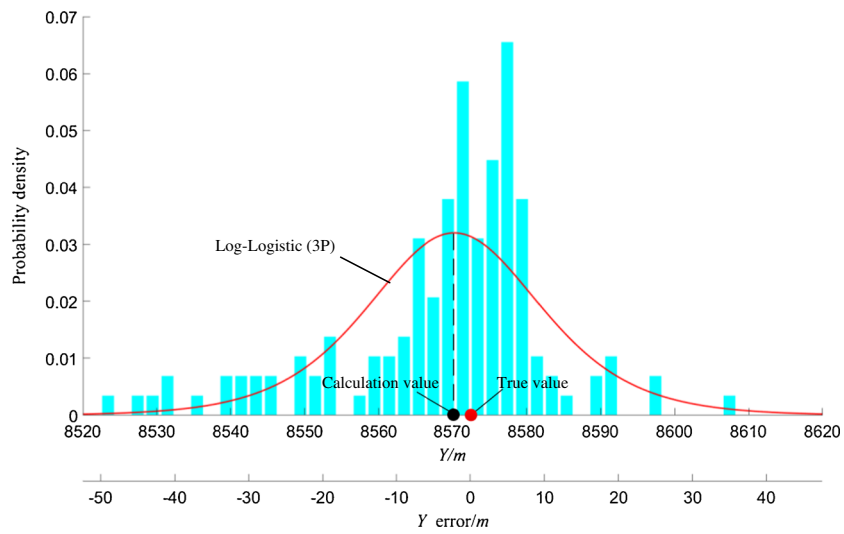
Discussion

The LM-VMD-SA method can obtain more stable MS source coordinates by combining the triggering sensors and fitting the location results of all sensor combination. The LM-VMD-SA method can degenerate to the ND-N method when 4 sensors are triggered for a MS event. Therefore, the superiority of the LM-VMD-SA method stands out when more than 4 sensors are triggered. Moreover, the velocity model database can also degenerate to a single uniform velocity model and layered velocity model for a homogeneous geological condition and layered geological conditions, respectively.

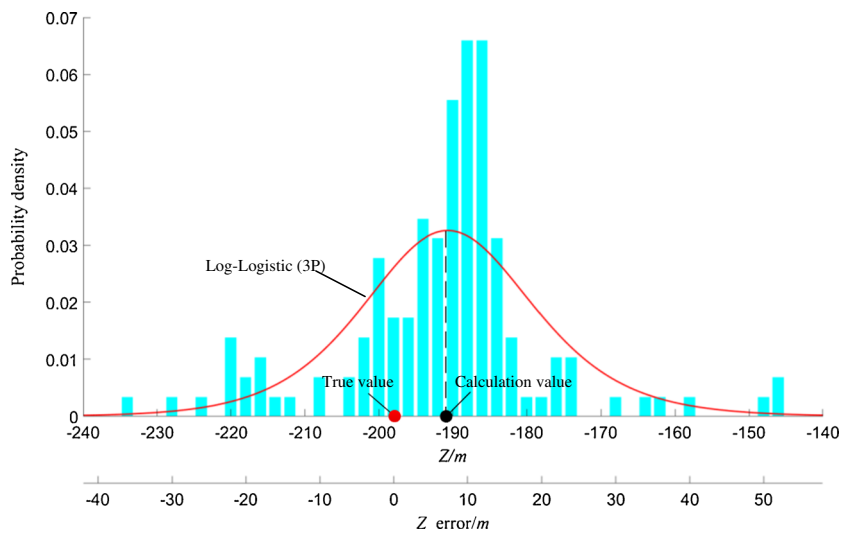
Since the number of sensor combinations is determined by $C_m^4 + C_m^5 + \dots + C_m^m$, more sensor combinations are acquired with the LM-VMD-SA method when more sensors are triggered. The relationship between the iteration time of the LM-VMD-SA method and the number of the sensor is studied, as shown in Fig. 13. It can be seen that the iteration time for event location in the LM-VMD-SA method increases with the increase of the number of triggering sensors. About 2.39s is required for blasting event location when the anisotropic velocity model proposed by Feng et al. (2017) is adopted in the Beiminghe Iron Mine. It can be concluded that the location



(a)



(b)



(c)

Fig. 9 Probability densities of 163 solutions and their errors and the fitting curves of blasting event No. 7 in the *x*-, *y*-, and *z*-coordinate directions using the log-logistic (3P) distribution probability density function. **a** *x*-coordinate direction. **b** *y*-coordinate direction. **c** *z*-coordinate direction

efficiency of the LM-VMD-SA method is higher than that of the anisotropic velocity model when the number of triggering sensors of the blasting event is less than 10. Due to the discrete sensor arrangement in the monitoring area of the Beiminghe Iron Mine, the triggered sensors are generally less than 10, so the LM-VMD-SA method can meet the requirements of rapid location.

Conclusions

A novel LM-VMD-SA method is proposed by improving the velocity model and the MS source location method, which is achieved by introducing a velocity model database and statistical analysis. Then, the effectiveness and robustness of the proposed method are verified. Some conclusions can be drawn as follows.

- (1) Based on the ND-N method and the pattern search algorithm, the LEOM-PSA method is proposed for inverting the optimal uniform velocity model and exhibits a good convergence.
- (2) An integrated method is proposed for creating and updating the velocity model database, where each sensor combination is assigned an optimal uniform velocity. Compared to the existing velocity models, the velocity model database considers the geological difference of

Fig. 10 Location results of the LM-VMD-SA method

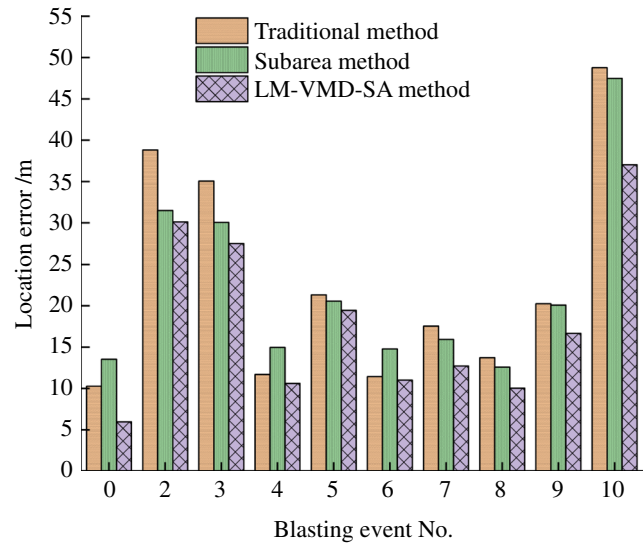
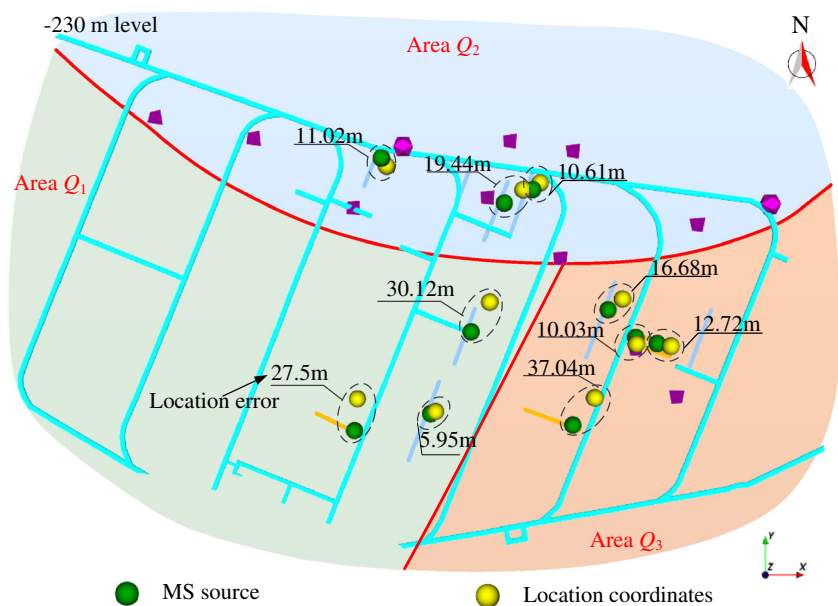
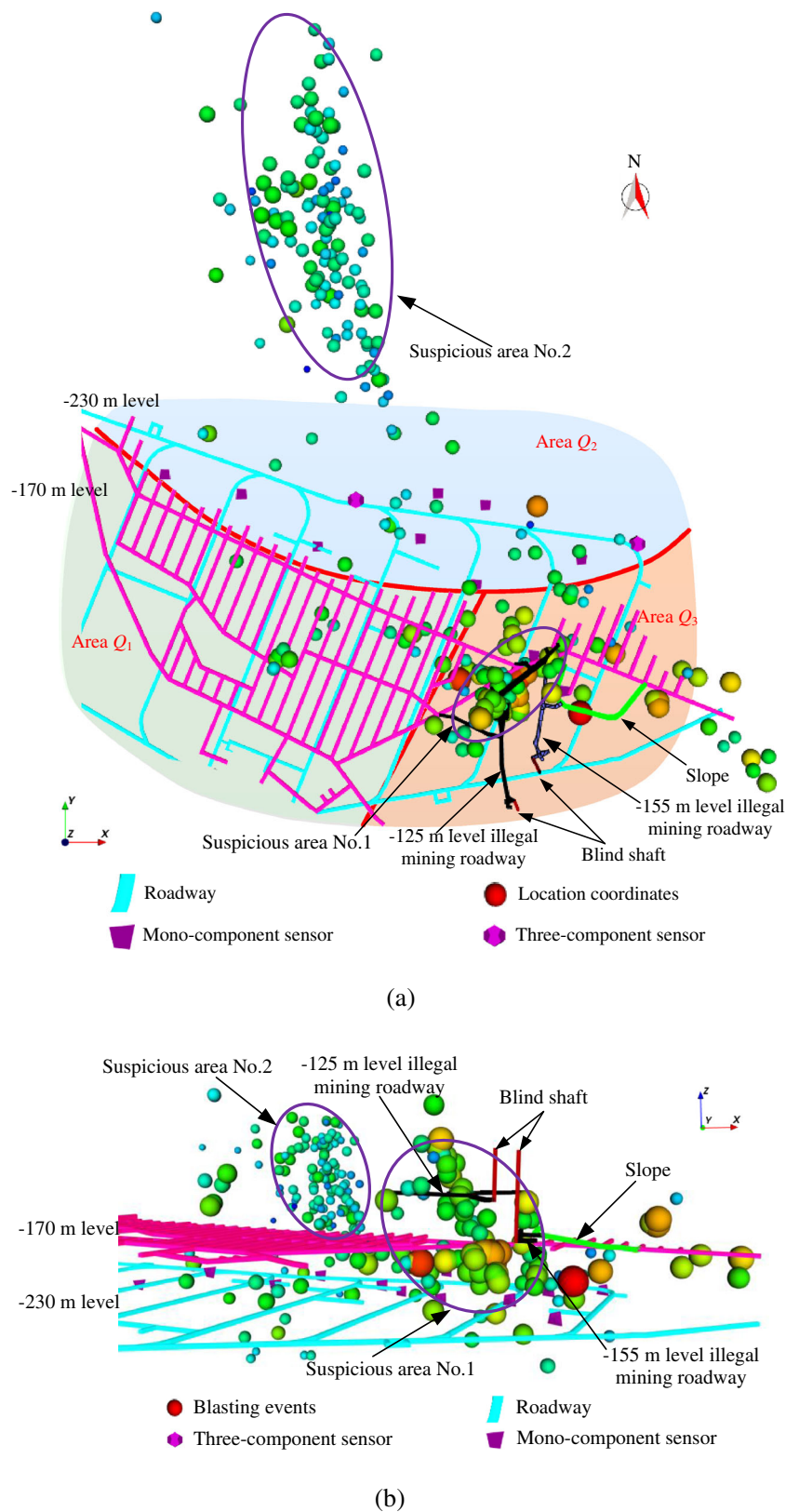


Fig. 11 Comparison of location errors of the traditional method, the subarea method, and the LM-VMD-SA method

several subareas and the monitoring area formed by the sensor combination, which is more fit with the actual conditions in mines.

- (3) The LM-VMD-SA method is proposed based on the velocity model database and the log-logistic (3P) distribution probability density function. With the proposed method, multiple location results of sensor combinations can be acquired, and the most accurate MS source coordinates are then determined by data analysis. Blasting tests in the Beiminghe Iron Mine show that the LM-VMD-SA method exhibits greater accuracy and solving stability than the traditional method and the subarea method.

Fig. 12 Locations of abnormal blasting events using the LM-VMD-SA method. **a** Top view. **b** Front view



(4) The application of the LM-VMD-SA method to the Beiminghe Iron Mine reveals that the concentrated abnormal blasting events are observed in the two

suspicious areas. In-site borehole information also verifies that there are illegal mining activities at the -125 m level and -155 m level and is completely

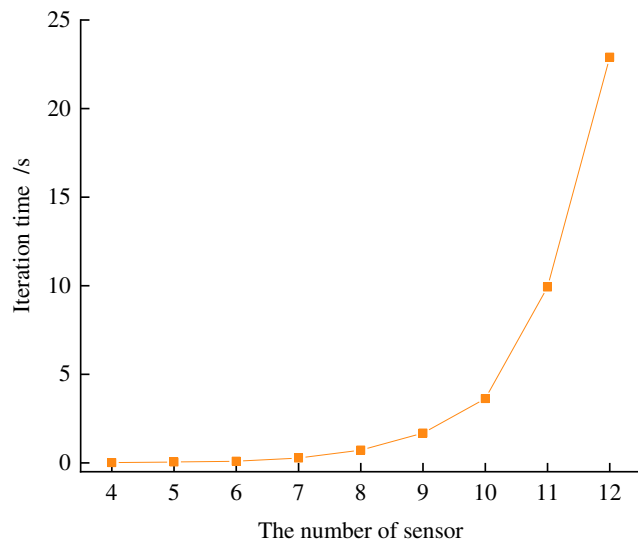


Fig. 13 The relationship between the iteration time of the LM-VMD-SA method and the number of the sensor

consistent with the position of the suspicious area No. 2.

Acknowledgements We would like to thank the staff at the Beiminghe Iron Mine of Minmetals Hanxing Mining Co., Ltd., in Hebei Province for their support and assistance in the field monitoring and data acquisition.

Funding This study received financial support from the National Natural Science Foundation of China (Grant No. 42077263, Grant No. 51539002) and the China Railway Corporation Science and Technology Research and Development Project (Grant No. P2019G001).

Declarations

Conflict of interest The authors declare that they have no competing interests.

References

- Adam L, Peter S (2009) Improvements in seismic event locations in a deep western U.S. coal mine using tomographic velocity models and an evolutionary search algorithm. *Min Sci Technol* 19(5):599–603. Available from: [https://doi.org/10.1016/S1674-5264\(09\)60111-3](https://doi.org/10.1016/S1674-5264(09)60111-3)
- Aki K, Christofferson A, Husebye ES (1977) Determination of the three-dimensional seismic structure of the lithosphere. *J Geophys Res* 82(2):277–296
- Crosson RS (1976) Crustal structure modeling of earthquake data 1. simultaneous least squares estimation of hypocenter and velocity parameters. *J Geophys Res* 81(17):3036–3046
- Crosson RS, Peters DC. (1974) Estimates of miner location accuracy: error analysis in seismic location procedures for trapped miners. *Seismic Detection and Location of Isolated Miners*
- Dai SH, Wang MO (1992) Reliability analysis in engineering applications. Van Nostrand Reinhold, New York
- Dong LJ, Hu QC, Tong XJ, Liu YF (2019) Velocity-free MS / AE source location method for three-dimensional hole-containing structures. *Engineering*. 6(7):827–834

- Dong LJ, Li XB, Ma J, Tang LZ (2017) Three-dimensional analytical comprehensive solutions for acoustic emission/microseismic sources of unknown velocity system. *Chin J Rock Mech Eng* 36(1):186–197
- Falls SD, Young RP (1998) Acoustic emission and ultrasonic-velocity methods used to characterise the excavation disturbance associated with deep tunnels in hard rock. *Tectonophysics*. 289(1–3):1–15
- Feng GL, Feng XT, Chen BR, Xiao YX (2017) A highly accurate method of locating microseismic events associated with rockburst development processes in tunnels. *IEEE Access* 5:27722–27731
- Feng GL, Feng XT, Chen BR, Xiao YX, Jiang Q (2015) Sectional velocity model for microseismic source location in tunnels. *Tunn Undergr Sp Technol* 45:73–83. Available from: <https://doi.org/10.1016/j.tust.2014.09.007>
- Geiger L (1912) Probability method for the determination of earthquake epicenters from arrival time only. *Bull Saint Louis Univ* 8:60–71
- Gesret A, Desassis N, Noble M, Romary T, Maisons C (2015) Propagation of the velocity model uncertainties to the seismic event location. *Geophys J Int* 200(1):52–66
- Grechka V, Duchkov AA (2011) Narrow-angle representations of the phase and group velocities and their applications in anisotropic velocity-model building for microseismic monitoring. *Geophysics*. 76(6):WC127–WC142
- Hirata A, Kameoka Y, Hirano T (2007) Safety management based on detection of possible rock bursts by AE monitoring during tunnel excavation. *Rock Mech Rock Eng* 40(6):563–576
- Lee WHK, Lahr JC. (1975) HYPO71, A computer program for determining hypocenter, magnitude, and first motion pattern of local earthquakes. *U.S. Geol. Surv. Open File Rept.* 75-311
- Li J, Li C, Morton SA, Dohmen T, Katahara K, Nafi TM (2013) Microseismic joint location and anisotropic velocity inversion for hydraulic fracturing in a tight Bakken reservoir. *Geophysics*. 79(5): C111–C122
- Li L, Tan JQ, Wood DA, Zhao ZG, Becker D, Lyu Q, Shu B, Chen H (2019) A review of the current status of induced seismicity monitoring for hydraulic fracturing in unconventional tight oil and gas reservoirs. *Fuel*. 242(January):195–210
- Li N, Ge MC, Wang EY (2014) Two types of multiple solutions for microseismic source location based on arrival-time-difference approach. *Nat Hazards* 73(2):829–847
- Li QP, Chen BR (2013) Research on micro-seismic source location during linear excavation process of deep tunnel. *The ISRM Commission on Design Methodology. Rock Characterisation, Modelling and Engineering Design Methods*, In: *Proceedings of the 3rd ISRM Sinorock Symposium*. Tongji Univ, Shanghai, China. p. 675–80.
- Li T, Cai MF, Cai M (2007) A review of mining-induced seismicity in China. *Int J Rock Mech Min Sci* 44:1149–1171
- Long Y, Liu JP, Lei G et al (2020) Progressive fracture processes around tunnel triggered by blast disturbances under biaxial compression with different lateral pressure coefficients. *Trans Nonferrous Metals Soc China* 30(9):2518–2535
- Lu CP, Liu GJ, Liu Y, Zhang N, Xue JH, Zhang L (2015) Microseismic multi-parameter characteristics of rockburst hazard induced by hard roof fall and high stress concentration. *Int J Rock Mech Min Sci* 76: 18–32
- Ma TH, Tang CA, Tang LX, Zhang WD, Wang L (2015) Rockburst characteristics and microseismic monitoring of deep-buried tunnels for Jinping II Hydropower Station. *Tunn Undergr Sp Technol* 49: 345–368
- Ma Y, Yuan C, Zhang J (2020) Joint microseismic event location and anisotropic velocity inversion with the cross double-difference method using downhole microseismic data. *Geophysics*. 85(3): KS63–KS73

- Milev A, Spottiswoode, Rorke A et al (2001) Seismic monitoring of a simulated rockburst on a wall of an underground tunnel. *J South Afr Inst Min Metall* 101(5):253–260
- Mooney WD, Laske G, Masters TG (1998) Crust 5.1: a global crustal model at $5^{\circ} \times 5^{\circ}$. *J Geophys Res* 103(1):727–747
- Mu WQ, Wang DY, Li LC, Yang TH, Feng QB, Wang SX, Xiao FK (2021) Cement flow in interaction rock fractures and its corresponding new construction process in slope engineering. *Constr Build Mater* 303(11):124533. <https://doi.org/10.1016/j.conbuildmat.2021.124533>
- Peng P, Wang L (2019) Targeted location of microseismic events based on a 3D heterogeneous velocity model in underground mining. *PLoS One* 14(2):1–18
- Poliannikov OV, Prange M, Malcolm AE, Djikpesse H (2014) Joint location of microseismic events in the presence of velocity uncertainty. *Geophysics*. 79(6):KS51–KS60
- Shang X, Li X, Morales-Esteban A, Chen G (2017) Improving microseismic event and quarry blast classification using artificial neural networks based on principal component analysis. *Soil Dyn Earthq Eng* 99(May):142–149. Available from. <https://doi.org/10.1016/j.soildyn.2017.05.008>
- Tang C, Li L, Xu N, Ma K (2015) Microseismic monitoring and numerical simulation on the stability of high-steep rock slopes in hydro-power engineering. *J Rock Mech Geotech Eng* 7(5):493–508
- Tezuka K, Niitsuma H (2000) Stress estimated using microseismic clusters and its relationship to the fracture system of the Hijiori hot dry rock reservoir. *Eng Geol* 56(1–2):47–62
- Wang HL, Ge MC (2008) Acoustic emission/microseismic source location analysis for a limestone mine exhibiting high horizontal stresses. *Int J Rock Mech Min Sci* 45(5):720–728
- Wang JQ, Jiang FX, Lü WS, Wang CW (2010) Microseismic wave propagation velocity insitu experiment and calculation. *J China Coal Soc* 35(12):2059–2063
- Wu LZ, Li SH, Huang RQ, Wang SY (2020) Micro-seismic source location determined by a modified objective function. *Eng Comput* 36(4):1849–1856
- Xiao PW, Li TB, Xu NW, Zhou Z, Liu X (2019) Microseismic monitoring and deformation early warning of the underground caverns of Lianghekou hydropower station, Southwest China. *Arab J Geosci* 12(16):496
- Xu NW, Li TB, Dai F, Li B, Zhu YG, Yang DS (2015) Microseismic monitoring and stability evaluation for the large scale underground caverns at the Houziyan hydropower station in Southwest China. *Eng Geol* 188:48–67
- Yang CX, Luo ZQ, Hu GB, Liu X (2007) Application of a microseismic monitoring system in deep mining. *J Univ Sci Technol Beijing* 14(1):6–8
- Yosef SS, Bruce AB (1994) Optimization by pattern search. *Eur J Oper Res* 78(3):277–303
- Zhu MB, Cheng JY, Wang LG (2019) The effect of P- and S-phase arrivals on the accuracy of microseismic source location. *J Appl Geophys* 164:130–139